Crystal structure of human mitoNEET reveals distinct groups of iron–sulfur proteins

Jinzhong Lin*†, Tao Zhou*, Keqiong Ye†‡, and Jinfeng Wang*‡

*National Laboratory of Biomacromolecules, Center for Structural and Molecular Biology, Institute of Biophysics, Chinese Academy of Sciences, Beijing 100101, China; and †National Institute of Biological Sciences, Beijing 102206, China

Edited by Richard H. Holm, Harvard University, Cambridge, MA, and approved July 15, 2007 (received for review March 16, 2007)

MitoNEET is a protein of unknown function present in the mitochondrial membrane that was recently shown to bind specifically the antidiabetic drug pioglizatone. Here, we report the crystal structure of the soluble domain (residues 32–108) of human mitoNEET at 1.8-Å resolution. The structure reveals an intertwined homodimer, and each subunit was observed to bind a [2Fe-2S] cluster. The [2Fe-2S] ligation pattern of three cysteines and one histidine differs from the known pattern of four cysteines in most cases or two cysteines and two histidines as observed in Rieske proteins. The [2Fe-2S] cluster is packed in a modular structure formed by 17 consecutive residues. The cluster-binding motif is conserved in at least seven distinct groups of proteins from bacteria, archaea, and eukaryotes, which show a consensus sequence of (hb)-C-X_1-C-X_2-(S/T)-X_3-P-(hb)-C-D-X_2-H, where hb represents a hydrophobic residue; we term this a CCCH-type [2Fe-2S] binding motif. The nine conserved residues in the motif contribute to iron ligation and structure stabilization. UV-visible absorption spectra indicated that mitoNEET can exist in oxidized and reduced states. Our study suggests an electron transfer function for mitoNEET and for other proteins containing the CCCH motif.

2Fe-2S | thiazolidinediones | mitochondria

Type 2 diabetes is a growing global health problem characterized by insulin resistance and pancreatic β-cell dysfunction (1). Thiazolidinediones (TZDs) are a class of insulin-sensitizing drugs used for treatment of type 2 diabetes (2), which includes rosiglitazone and pioglitazone currently in clinic use. The mechanism of action of TZDs has been generally attributed to their direct activation of peroxisome proliferator-activated receptor-γ, a ligand-binding nuclear receptor important for adipocyte differentiation and glucose homeostasis (3). However, accumulating evidence suggests that TZDs may also exert effects via a peroxisome proliferator-activated receptor-γ-independent pathway, particularly through modulation of mitochondrial activity (4–6). Colca *et al.* (7) have recently identified a protein in the mitochondrial membrane that crosslinks with photo-affinity-labeled pioglitazone (7). The crosslink could be competed by unlabeled pioglitazone, suggesting specificity in TZD binding. The protein was named mitoNEET because of its mitochondrial location and because of the presence of the sequence motif Asn-Glu-Glu-Thr ("NEET"). MitoNEET has a putative N-terminal transmembrane helix, which likely serves as a membrane anchor, and several invariant cysteine and histidine residues, which suggests that mitoNEET contains a CDGSH-type zinc finger (Fig. 1). However, its sequence is not homologous to any protein or domain of known function. Elucidation of the function and structure of mitoNEET is important to reveal its biological activity, to understand the pharmacology of TZDs, and to aid in the design of more potent antidiabetic drugs. Here, we show by structural characterization that mitoNEET is a previously unrecognized iron–sulfur protein, suggesting a role in electron transfer. We also define seven groups of proteins that contain the same cluster-binding motif.

Results

Structure Determination. The full-length human mitoNEET protein (108 residues) was insoluble when expressed in *Escherichia coli*; however, a fragment (residues 32–108) missing the putative N-terminal transmembrane helix showed high solubility. The soluble fragment was used in all of the following structural and biochemical studies and is simply referred to as mitoNEET hereafter. The expression of the fragment depended critically on the presence of iron ions in the minimal M9 media. Moreover, the protein solution and crystals displayed a reddish color [supporting information (SI) Fig. 5*A*]. Thus, we suspected that mitoNEET is an iron-binding protein, and we treated the x-ray diffraction data collected at 1.54 Å as having anomalous signals from iron. Indeed, prominent anomalous scattering centers were identified. The structure was determined using the single-wavelength anomalous dispersion technique. The electron density map showed rhombus-shaped density around scattering centers, characteristic of a [2Fe-2S] cluster (SI Fig. 5*B*). The structure has been refined to 1.8-Å resolution and has an R_{free} factor of 19.3% and an R factor of 16.4% (SI Table 1). The overall coordinate error was estimated to be ≈0.11 Å, which is based on the R_{free} value.

Overall Structure. The crystal structure reveals that mitoNEET is a homodimer with each subunit binding a [2Fe-2S] cluster (Fig. 2*A*). The dimeric structure adopts a globular fold, resembling a vase of 37 Å in height. The bottom half of the structure, or "body," is ≈35–38 Å in diameter, and the upper half, or "neck," is ≈20 Å in diameter. The [2Fe-2S] cluster is bound within a loop region in the body, close to the neck–body boundary.

The two monomer structures are almost identical and can be superimposed with a rms deviation of 0.091 Å over 64 Cα pairs. Each monomer comprises three β-strands (β1, β2, and β3), one α-helix (α1), and four loops (L1, L2, L3, and L4), which are arranged in the order L1-β1-L2-β2-L3-α1-L4-β3 (Fig. 2*B*). Loop L2, which connects strands β1 and β2, harbors a short 3_{10}-helix. The body part would be tethered to the membrane by the two N-terminal transmembrane helices, which are missing in the structure of the soluble fragment (Fig. 2*C*).

The structure of mitoNEET is distinct from other iron–sulfur proteins that have been characterized to date. Moreover, no structural homolog ($Z > 0.5$) could be found in the current Protein Data Bank when either the monomeric or dimeric structure was used in a DALI search (8), suggesting that the structure represents a previously unrecognized fold.

Author contributions: J.L., K.Y., and J.W. designed research; J.L., T.Z., and K.Y. performed research; J.L., K.Y., and J.W. analyzed data; and J.L., K.Y., and J.W. wrote the paper.

The authors declare no conflict of interest.

This article is a PNAS Direct Submission.

Abbreviations: TZD, thiazolidinedione; GltS-FMN, glutamate synthase FMN-binding domain.

Data deposition: The atomic coordinates of the mitoNEET structure have been deposited in the Protein Data Bank, www.pdb.org (PDB ID code 2QD0).

‡To whom correspondence may be addressed. E-mail: jfw@sun5.ibp.ac.cn or yekeqiong@nibs.ac.cn.

This article contains supporting information online at www.pnas.org/cgi/content/full/0702426104/DC1.

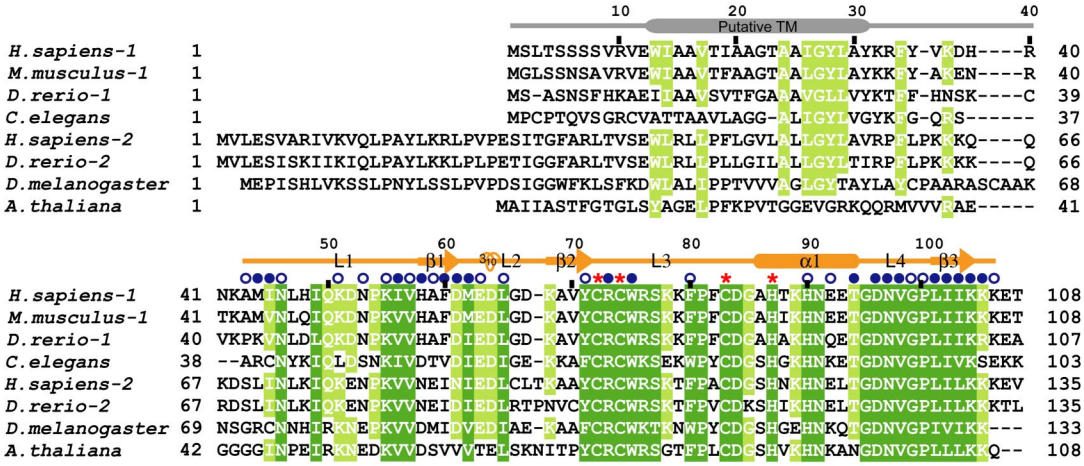

Fig. 1. Multiple sequence alignment of mitoNEET homologs. Aligned are sequences from *Homo sapiens* (1, NP_060934; 2, NP_001008389), *Mus musculus* (1, NP_598768; 2, not shown), *Danio rerio* (1, NP_956899; 2, NP_956677), *Drosophila melanogaster* (NP_651684), *Caenorhabditis elegans* (NP_0010022387), and *Arabidopsis thaliana* (NP_568764). The first sequence is mitoNEET used in this study. Secondary structure elements observed in the crystal structure and a predicted transmembrane helix (TM) are shown at the top. Shown are residues whose surface area is buried by at least 30 Å^2 (●) and 10 Å^2 (○) due to dimerization. Asterisks denote iron-coordinating ligands. Residues with 100% and 70% conservation are shaded by dark and light green colors, respectively.

Dimer Formation. The monomer subunits associate with each other along their full length to form an intertwined structure with an extensive interface. The neck part comprises a β-sandwich that is formed by two three-stranded intermolecular β-sheets (Fig. 2*A*). Each β sheet consists of strand β1 from one subunit and strands β2′ and β3′ from the other subunit (prime denotes the other subunit), which are arranged in the order β1-β3′-β2′. Hence, two β1 strands are swapped between the two β-sheets. Strands β1 and β3′ run parallel to each other, and strands β2′ and β3′ are antiparallel. The β-sandwich contains a hydrophobic core comprising conserved residues Phe-60, Met-62, Leu-65, Ala-69, Tyr-71, Leu-101, and Ile-103 from both subunits. In the body part, loops L1 and L3 from one subunit associate with loops L4′ and L3′ from the other subunit. The association is stabilized by a large number of intermolecular hydrogen bonds and two symmetric hydrophobic cores, one of which comprises residues Ile-45, Ile-56, Trp-75, Phe-80, and Val-98′. Overall, the extensive dimer interface involves 53% of structured residues and buries a solvent-accessible surface area of 1,988 Å^2 per monomer, which accounts for ≈36% of the total surface area of a monomer (Fig. 1). The conservation of the dimer interface suggests that all mitoNEET homologs fold into a similar dimeric structure (Fig. 2*C*).

There are patches of conserved residues on the surface of the molecule (Fig. 2*D*). One patch comprising residues Leu-102, Lys-55′, and Val-57′ is near the opening of the iron–sulfur cluster at the subunit junction. Another patch comprising Glu-63 and Asp-64 is located at the tip. These exposed, conserved regions may be functionally important sites.

Structure of [2Fe-2S] Binding Module. In the mitoNEET structure, each [2Fe-2S] cluster is bound within a stretch of 17 consecutive residues (residues 71–87) from loop L3 and the N terminus of helix α1. The polypeptide chain makes a full turn and sandwiches the cluster between the two ends of the 17-aa stretch, forming a compact, knot-like structure. The [2Fe-2S] cluster is composed of two iron atoms (Fe1, Fe2) and two bridging sulfur atoms (S1, S2) located in the same plane and is largely buried with Fe2 facing into the solvent. Loop L4 partially shields the opening of the cluster.

The [2Fe-2S] cluster is coordinated by three cysteines and one histidine with the buried Fe1 atom bound by Cys-72 and Cys-74 and with the exposed Fe2 atom bound by Cys-83 and His-87 (Fig. 3*A*). Iron–sulfur clusters are usually bound by four cysteines, although noncysteinyl residues, such as histidine, aspartate, serine, or backbone amide occasionally serve as ligands (9). In Rieske-type clusters, Fe1 is coordinated by two cysteines, and Fe2 is coordinated by two histidines (10). In mitoNEET, Fe2 is asymmetrically coordinated by one cysteine and one histidine, which to the best of our knowledge represents a previously unrecognized, naturally occurring coordination pattern for a [2Fe-2S] cluster, although a Rieske-type protein has been successfully engineered to contain three cysteines and one histidine ligands (11). Histidine ligation has been proposed to result in unique redox and spectroscopic properties of Rieske-type clusters and to couple proton and electron transport (12–14). It remains to be seen how the single histidine ligation in mitoNEET influences the properties of the iron–sulfur cluster and thus protein function.

It is remarkable that all four [2Fe-2S] ligands in mitoNEET are contained within a small modular unit comprising only 17 residues. In other [2Fe-2S] binding proteins, iron ligands are normally distributed in discrete regions of primary sequence (12, 15, 16). Plant-type and vertebrate-type [2Fe-2S] ferredoxins have a consensus cluster-binding sequence of C-$X_{4/5}$-C-X_2-C . . . C, which has three cysteine ligands close in sequence and a fourth one that is separated in sequence (3 + 1 pattern). The cluster-binding sequence in Rieske proteins shows a 2 + 2 pattern (C-X-H . . . C-X_2-H) with two separated pairs of cysteine and histidine residues. These [2Fe-2S] binding regions are generally part of larger structures, in contrast with the compact cluster binding module of mitoNEET.

The Cys-3-His-1-coordinated [2Fe-2S] cluster adopts a standard rhombic geometry, with Fe1 and Fe2 2.75 Å apart and the length of the Fe-S bond in the range 2.20–2.23 Å, like other Cys-4- or Cys-2-His-2-coordinated clusters (SI Table 2). Fe1 is coordinated by sulfur atoms S1, S2, Cys72Sγ, and Cys74Sγ in a nearly ideal tetrahedral arrangement with bond angles of 101–116°. The plane defined by Cys72Sγ-Fe1-Cys74Sγ is almost perpendicular to the plane of the [2Fe-2S] cluster. In contrast, the coordination sphere of Fe2 shows a distorted tetrahedral symmetry, apparently due to the asymmetric ligation by cysteine and histidine. With respect to the Cys72Sγ-Fe1-Cys74Sγ plane, the His78Nδ-Fe2-Cys83Sγ plane is rotated by ≈13° around the Fe1-Fe2 vector. In both Cys-4- and Cys-2-His-2-coordinated

BIOCHEMISTRY

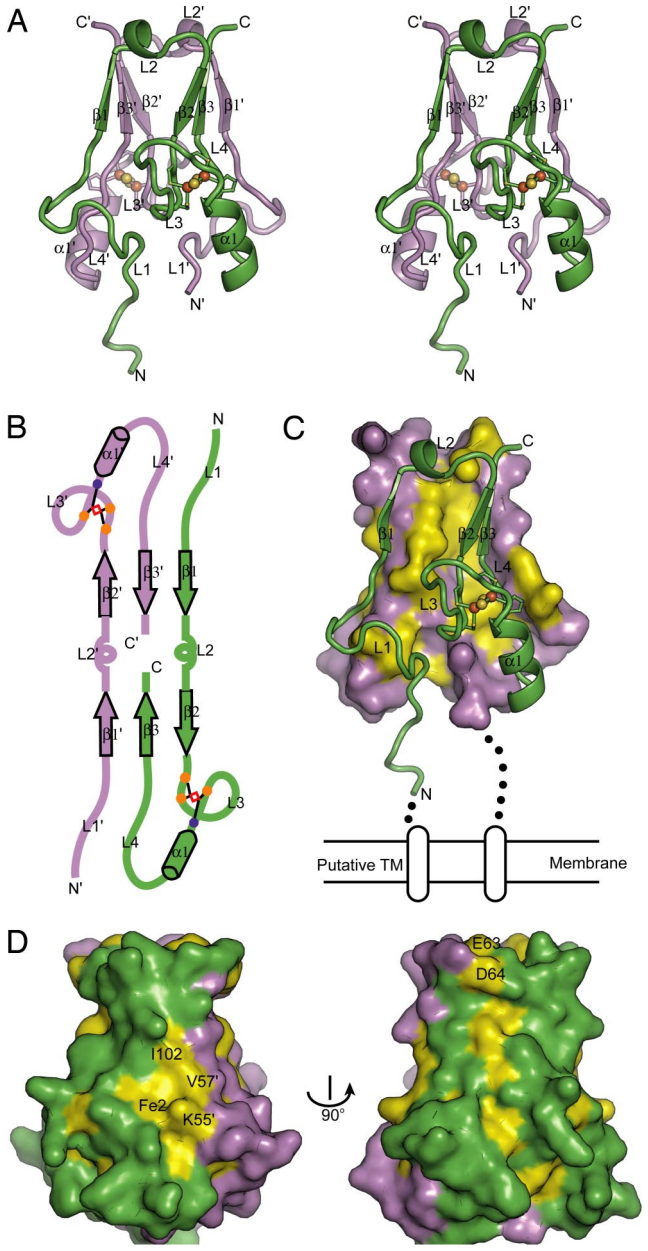

Fig. 2. Crystal structure of the soluble domain of human mitoNEET. (*A*) Crosseye stereoview of the ribbon representation of the structure. The two monomer subunits are colored green and violet, respectively. The [2Fe-2S] cluster and ligand residues are represented as balls and sticks. Iron and sulfur atoms are colored orange and yellow, respectively. The secondary structure elements and N and C termini are labeled, with prime denoting the violet subunit. (*B*) Topology diagram of the intertwined dimer. Cysteine and histidine ligands are shown as orange and blue spots, and [2Fe-2S] clusters are shown as red rhombi. (*C*) The dimerization interface with the violet subunit is shown as surface representation, and the green subunit is shown as ribbons. The most highly conserved residues are colored in yellow in the violet subunit. Also shown is the relative orientation of the membrane. (*D*) The most highly conserved residues on the molecular surface are shown as yellow patches.

[2Fe-2S] clusters, the four coordinating atoms (Sγ or Nδ) and two Fe atoms are located almost in the same plane.

Each of the three cysteine Sγ atoms and two bridging inorganic sulfur atoms that ligate Fe form one or two hydrogen bonds with backbone amide groups (Fig. 3*A*). In other iron–sulfur proteins, the Sγ atom of cysteine i commonly forms a hydrogen bond with the amide group of residue i + 2 (16). Such a hydrogen-bonding pattern also exists in Cys-72, Cys-74, and Cys-83 of mitoNEET (Fig. 3*A*).

CCCH-type [2Fe-2S] Binding Motif. The 17-residue [2Fe-2S] binding motif can be found in hundreds of proteins from a wide range of organisms including bacteria, archaea, and eukaryotes (Fig. 4), with a consensus sequence of (hb)-C-X_1-C-X_2-(S/T)-X_3-P-(hb)-C-D-X_2-H, where hb stands for one of hydrophobic residues Leu, Ile, Met, Val, Phe, Tyr and Trp, and X_n means a stretch of n residues of arbitrary type. This motif has been previously annotated as a CDGSH-type zinc finger [SMART database accession no. SM00704 (17)]. In light of the mitoNEET structure, we propose renaming the consensus sequence as a CCCH-type [2Fe-2S] binding motif to reflect the unique ligation pattern of the [2Fe-2S] cluster.

The motif is characterized by nine conserved core residues with invariant spacing between them. The core residues of human mitoNEET include four ligand residues, Cys-72, Cys-74, Cys-83, and His-87, and five nonligand residues, Tyr-71, Ser-77, Pro-81, Phe-82, and Asp-84. Although the role of the ligand residues in the [2Fe-2S] cluster coordination is apparent, the mitoNEET structure reveals that the nonligand residues critically stabilize the cluster-binding, knot-like structure (Fig. 3*A*). Residues Ser-77 and Asp-84 are conserved because their side chains make bridging contacts with backbone atoms. Ser77Oγ makes bifurcate hydrogen bonds with Lys79N and Phe82O, and Asp-84 simultaneously interacts with Lys78N and Ala86N through two carboxyl oxygen atoms. The threonine substitution of Ser-77 observed in some CCCH motif sequences probably preserves the hydrogen bonds formed by the hydroxyl group. Residues Tyr-71, Pro-81, and Phe-82 form a small hydrophobic core, which interacts with the hydrophobic core of the β sandwich. Pro-81 also contributes to the formation of a turn structure. Conservation of these structurally important core residues strongly suggests that all CCCH-type sequences fold into a modular [2Fe-2S] binding structure.

In the mitoNEET structure, most noncore residues project outwards into the solvent or contact with surrounding structures. Noncore residues Arg-73, Trp-75, Arg-76, and Phe-80 make contact with loops L1, L4′, and L3′ (Fig. 3*B*). Trp-75 and Phe-80 form a hydrophobic core with Ile-45, Ile-56, and Val-98′. The indole ring of Trp-75 (Nε) also forms a hydrogen bond with Arg-73′O. Notably, residue Arg-73′ (i.e., from the other subunit as shown in Fig. 3*B*) is totally buried at the dimer interface, with its guanidine group forming three hydrogen bonds with Pro-100′O, Ile56O, and a buried water, which also interacts with Cys72O and Pro81O. Arg-76 interacts with a carbonyl oxygen atom (Fig. 3*B*). Because of their involvement in interactions within the structure, these four noncore residues are highly conserved among mitoNEET homologs, whereas other noncore residues are exposed to the solvent and are less well conserved (Fig. 1).

CCCH Motif-Containing Proteins. Proteins containing the CCCH motif can be divided into seven groups according to the number and arrangement of the CCCH motifs and their overall sequence homology (Fig. 4). Proteins belonging to the same group share sequence homology over an extended range and are likely to have a related function. Proteins in the different groups show no significant sequence homology beyond the CCCH motif.

Group 1 includes close homologs of mitoNEET that are present in metazoans and higher plants (Fig. 1). They are often present as two copies in vertebrates and as a single copy in other organisms. The longer version (protein 2 in Fig. 1) of the two vertebrate copies has a ≈30-residue extension upstream of the putative transmembrane helix. Interestingly, the longer human version of the protein is found localized in the endoplasmic reticulum (18). The single copy in other organisms may be the

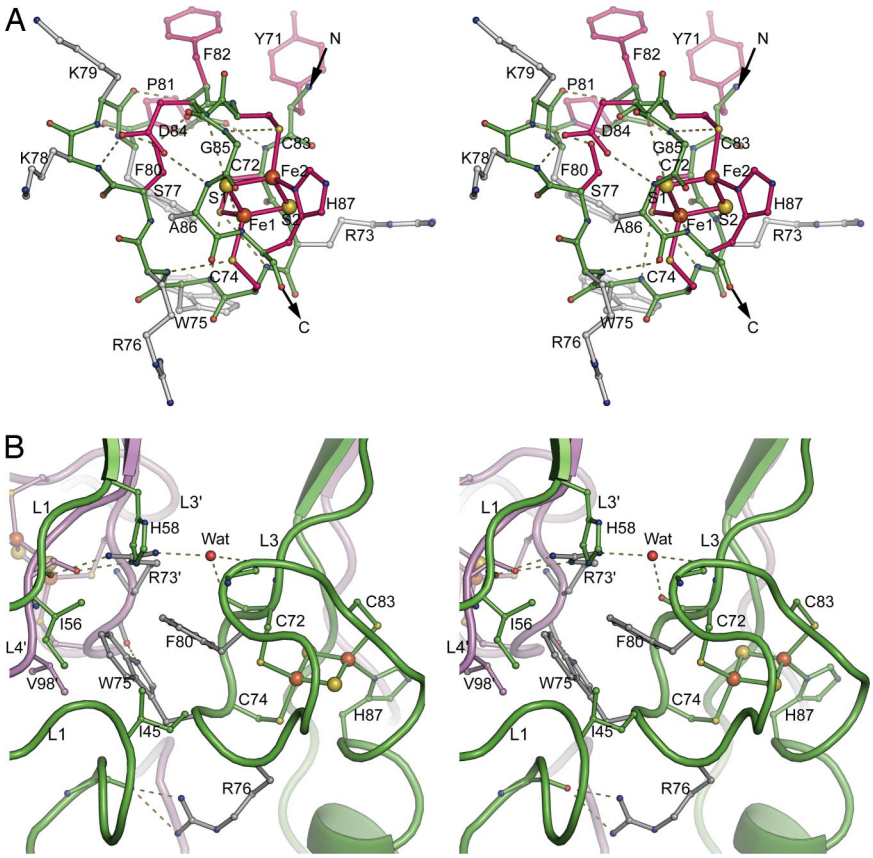

Fig. 3. Structure of the [2Fe-2S] binding module in crosseye stereoview. (*A*) Stick and ball representation of the module. Backbone bonds are colored green, side chains of the core residues are pink, and side chains of noncore residues are gray. Nitrogen atoms are colored blue, oxygen atoms are colored red, sulfur atoms are colored yellow, and iron atoms are colored orange. Dashes stand for hydrogen bonds. (*B*) Interaction of the noncore residues with the structural environment. The two monomer subunits are colored green and violet, respectively.

longer version, for example in flies, or the shorter version, as found in worms. All mitoNEET homologs share the highly conserved soluble domain, but the homologs in the higher plants arabidopsis and rice appear to lack the transmembrane helix.

A single CCCH motif can be identified in protein sequences from a few *Apicomplexa*, including malaria-causing *Plasmodium* (group 2), archaea (group 3), and bacteria (group 4). The *Apicomplexa* sequences are closely related with mitoNEET in the noncore residues and even at regions outside the motif, but the bacterial and archaeal sequences show no significant homology with mitoNEET other than the core residues of the CCCH motif.

The CCCH motif exists as two copies in a large number of sequences that can be classified into groups 5, 6, and 7. In group 5, which comprises exclusively bacterial sequences, the tandem repeats are spaced by ≈20 aa residues and are followed by a glutamate synthase FMN-binding domain (GltS-FMN). The GltS-FMN domain catalyzes the conversion of 2-oxoglutarate into L-glutamate, which requires electron donation from a noncovalently bound ferredoxin or NAD(P)H (19). Electrons are transferred to a reaction intermediate through a FMN cofactor and a [3Fe-4S] cluster in the GltS-FMN domain. The tandem [2Fe-2S] clusters preceding the GltS-FMN domain in group 5 proteins probably participate in the same electron transfer process. Interestingly, eukaryotic and bacterial organisms have short proteins (group 6) that contain only tandem repeats highly similar to those in group 5, but do not contain the GltS-FMN domain.

Some archaeal and bacterial sequences (group 7) contain two CCCH repeats conjugated to a functionally unknown PUF1271 domain in a variable arrangement. The DUF1271 domain can be flanked by two CCCH repeats or can be located upstream of one or two repeats. DUF1271 is also present as a stand-alone, single-domain protein or as connected to other domains. There are also orphan CCCH-containing proteins that could not be readily categorized because there are too few examples.

On the whole, these CCCH motif-containing sequences from different groups share core residues that are important for forming the modular [2Fe-2S] binding structure. Members within a group often have a conserved subset of noncore residues (Fig. 4), which probably reflects the packing constraints imposed by different structural environments.

Discussion

In this study, we determined the crystal structure of a soluble domain of mitoNEET and showed that mitoNEET is a type of iron–sulfur protein rather than a zinc-finger protein as previously predicted. The [2Fe-2S] binding module features a unique coordination pattern of three cysteines and one histidine and a highly compact structure comprising only 17 consecutive residues. Iron–sulfur clusters, which are mainly of [2Fe-2S], [4Fe-4S], and [3Fe-4S] types, are ubiquitous protein cofactors that function primarily in electron transfer and also in other diverse processes such as substrate binding, gene regulation, and oxygen/nitrogen-sensing events (9, 20–22). Iron–sulfur clusters transfer one electron at a time by alternating the oxidized and reduced states of one iron. The UV-visible absorption spectra of mitoNEET changed reversibly in the oxidized and reduced states

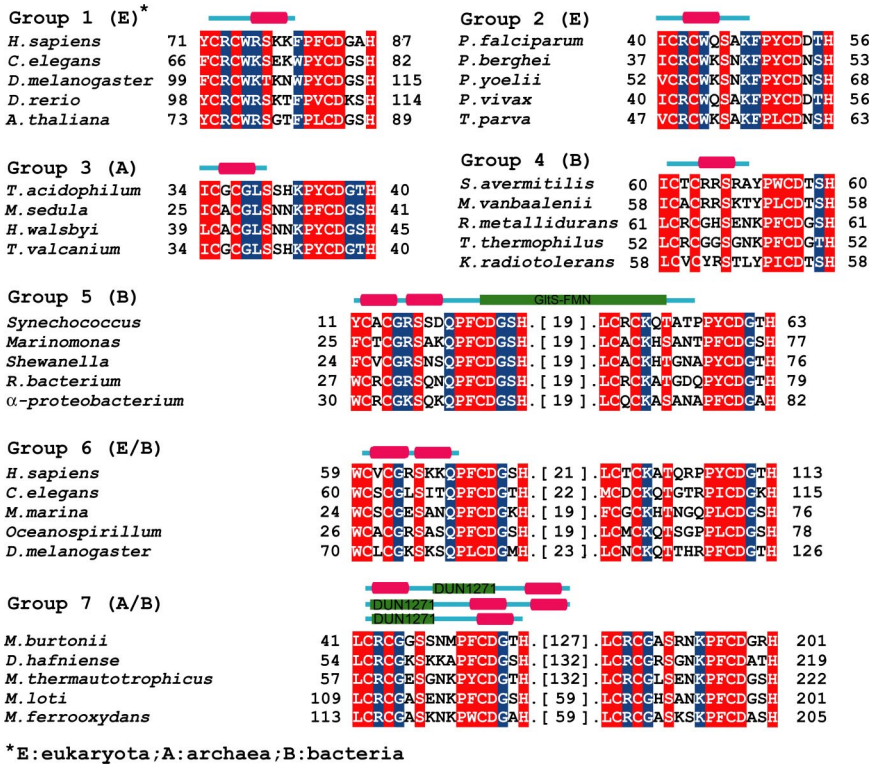

Fig. 4. The seven groups of CCCH motif-containing proteins. The 17-residue [2Fe-2S] binding motif sequences are aligned with the universally conserved core residues shaded in red, and the noncore residues that are conserved only within an individual group are shaded in blue. The domain arrangements of each group are indicated with the CCCH motif as a magenta box. Group 7 has a variable domain arrangement. Each sequence is indicated by the name of species from which it originates. The numbers of the starting and ending residues are indicated, as are the numbers of omitted residues between tandem CCCH repeats. The accession numbers of the sequences in the order of the alignment are as follows: NP_060934, NP_001022387, NP_651684, NP_956677, and NP_568764 in group 1; NP_473158, XP_669761, XP_730809, AAF99457, and XP_764182 in group 2; NP_393562, ZP_01600028, YP_658160, and NP_110689 in group 3; NP_828371, YP_956561, YP_586540, YP_005939, and ZP_00619216 in group 4; ZP_01083369, ZP_01074254, ZP_00837134, ZP_01015104, and ZP_01446837 in group 5; EAW60525, NP_497419, ZP_01694071, ZP_01167744, and NP_6101234 in group 6; and YP_565248, YP_516858, NP_275341, NP_105478, and ZP_01452291 in group 7.

(SI Fig. 6), which is consistent with mitoNEET's role as an electron carrier. The mitoNEET dimer contains two [2Fe-2S] clusters separated by ≈12 Å, a distance that in principle could allow electrons to hop between clusters. It is also possible that the two clusters simultaneously participate in a two-electron transfer process.

Human mitoNEET is localized in mitochondria as shown by the colocalization of green fluorescence protein-fused mitoNEET and MitoTracker (SI Fig. 7). Mitochondria harbor a large number of iron–sulfur proteins that transfer electrons as part of the respiratory chain or in various oxidation reduction processes. The specific function of mitoNEET remains to be studied. Nevertheless, our results suggest that mitoNEET may be involved in an unidentified electron transport pathway. The expression level of mitoNEET is substantially increased when preadipocytes differentiate into adipocytes (7). MitoNEET depletion by siRNA treatment significantly enhances lactate production in astrocytes (5). These studies suggest that mitoNEET has a metabolic role. The future challenge will be to reveal the metabolic pathway that involves mitoNEET and to reveal how pioglitazone modulates that pathway. In a modeling effect, we observed that pioglizaone could be docked in a deep groove on the mitoNEET surface near the iron-sulfur cluster (SI Fig. 8); such interaction might interfere with the binding of mitoNEET with an endogenous substrate. However, the exact binding mode and the existence of such a substrate remain to be investigated.

Our structure also allowed definition of a CCCH-type of [2Fe-2S] binding motif that is found in seven distinct groups of proteins. Identifying the likely presence of [2Fe-2S] clusters in these proteins will greatly facilitate their functional characterization.

Materials and Methods

Protein Expression and Purification. The human mitoNEET gene (gene symbol: *ZCD1*) was PCR amplified from a human liver cDNA library. A fragment containing residues 32–108 was cloned into the pET-28b vector (Novagen, San Diego, CA). The protein contains an N-terminal, thrombin-cleavable six-His-tag derived from the vector. Protein expression in *E. coli* BL21(DE3) cells was auto-induced at 37°C as described in ref. 23.

The cell pellets were lysed by sonication in buffer A (20 mM Tris·HCl, pH 7.9/5 mM imidazole/500 mM NaCl). The clarified supernatant was loaded onto a Ni-NTA column preequilibrated with buffer A. The column was then washed with 5-column volumes of buffer A and with 5-column volumes of buffer A containing 30 mM imidazole and then reequilibrated with the thrombin cleavage buffer (50 mM Tris·HCl, pH 7.5/150 mM NaCl/2.5 mM $CaCl_2$). The mitoNEET soluble domain was released by on-column thrombin cleavage of the His-tag for 16 h at room temperature and was eluted with buffer A containing 30 mM imidazole. The protein was further purified by gel filtration chromatography (Sephadex G-50) in 20 mM Tris·HCl, pH 8.0, and concentrated to 20 mg/ml.

Crystallization and Structure Determination. The crystals were grown by the hanging-drop vapor diffusion method at 20°C. Two isomorphic crystals obtained under two crystallization conditions were used in structure determination. Crystal 1 was grown

by mixing 2 μl of protein solution (20 mg/ml in 20 mM Tris·HCl buffer, pH 8.0) and 2 μl of well solution containing 100 mM Tris·HCl (pH 7.4), 18% PEG 3350, and 200 mM potassium iodide. Crystal 2 was grown in 100 mM Tris·HCl (pH 7.2), 30% PEG 2000, and 100 mM NaCl. For cryoprotection, glycerol was added into the crystallization drop in 5% increments up to 15% (vol/vol), and the drop was equilibrated for 5 min in each step. Crystals were then flash frozen in liquid nitrogen until use. Diffraction data of crystal 1 were collected to a 2.2-Å resolution at the wavelength of 1.5418 Å with a Rigaku (Tokyo, Japan) machine, and the crystal 2 data were collected to 1.8 Å at the wavelength of 1.0 Å at Japan SPring-8 beamline BL41XU.

The diffraction data were processed and scaled using Denzo and Scalepack (24). Both crystals were isomorphic, belonging to the primitive orthorhombic space group $P2_12_12_1$ (a = 65.971 Å, b = 43.838 Å, c = 59.139 Å). The asymmetric unit contained one dimer molecule. The structure was determined based on the 2.2 Å data by the single-wavelength anomalous dispersion method making use of the intrinsic anomalous signals from iron. Four heavy atom positions were identified using the program Shelxd (25) and were used to calculate the initial phases that were further improved by density modification in CNS1.1 (26). The resulting electron density map was of excellent quality. The model was built in Coot (27). Refinement was carried out using either CNS1.1 or REFMAC with 20 TLS groups (28). The final model refined against the 1.8 Å data includes residues 43–106 for one subunit, residues 38–106 for the other subunit, two [2Fe-2S] clusters, and 100 water molecules. The structured N-terminal tail (residues 38–42) of the later subunit participates in the crystal packing interactions. In the Ramachandran plot (29), 87.8% of nonglycine and nonproline residues were in the most favored regions, and 12.2% of these residues were in additional allowed regions.

Note Added in Proof. After we submitted our paper, Dixon and coworkers (30) showed that mitoNEET is an iron-containing, mitochondrial, outer membrane protein that regulates oxidative capacity. Dixon and coworkers (31) recently also showed by biochemical analysis that mitoNEET contains a redox-active [2Fe–2S] cluster coordinated by three cysteine residues and one histidine residue.

We thank Lei Yin for assistance in the preliminary crystal screen; N. Shimizu and M. Kawamoto for help at SPring-8 beamline BL41XU; and Prof. S. Perrett at the Institute of Biophysics for editing this manuscript and for helpful suggestions. J.W. was supported by Grant 2002BA711A13 from the 863 Special Program of China and Grant KSCX1-SW-17 from the Knowledge Innovation Project of the Chinese Academy of Sciences. K.Y. was supported by the Ministry of Science and Technology.

1. Leahy JL (2005) *Arch Med Res* 36:197–209.
2. Yki-Jarvinen H (2004) *N EnglJ Med* 351:1106–1118.
3. Semple RK, Chatterjee VK, O'Rahilly S (2006) *J Clin Invest* 116:581–589.
4. Furnsinn C, Waldhausl W (2002) *Diabetologia* 45:1211–1223.
5. Feinstein DL, Spagnolo A, Akar C, Weinberg G, Murphy P, Gavrilyuk V, Dello Russo C (2005) *Biochem Pharmacol* 70:177–188.
6. Colca JR, Kletzien RF (2006) *Exp Opin Invest Drugs* 15:205–210.
7. Colca JR, McDonald WG, Waldon DJ, Leone JW, Lull JM, Bannow CA, Lund ET, Mathews WR (2004) *Am J Physiol* 286:E252–E260.
8. Holm L, Sander C (1993) *J Mol Biol* 233:123–138.
9. Johnson DC, Dean DR, Smith AD, Johnson MK (2005) *Annu Rev Biochem* 74:247–281.
10. Ferraro DJ, Gakhar L, Ramaswamy S (2005) *Biochem Biophys Res Commun* 338:175–190.
11. Kounosu A, Li Z, Cosper NJ, Shokes JE, Scott RA, Imai T, Urushiyama A, Iwasaki T (2004) *J Biol Chem* 279:12519–12528.
12. Link TA (1999) *Adv Inorg Chem* 47:83–157.
13. Mason JR, Cammack R (1992) *Annu Rev Microbiol* 46:277–305.
14. Berry EA, Guergova-Kuras M, Huang LS, Crofts AR (2000) *Annu Rev Biochem* 69:1005–1075.
15. Sticht H, Rosch P (1998) *Prog Biophysics Mol Biol* 70:95–136.
16. Iwata S, Saynovits M, Link TA, Michel H (1996) *Structure (London)* 4:567–579.
17. Letunic I, Copley RR, Pils B, Pinkert S, Schultz J, Bork P (2006) *Nucleic Acids Res* 34:D257–D260.
18. Simpson JC, Wellenreuther R, Poustka A, Pepperkok R, Wiemann S (2000) *EMBO Reports* 1:287–292.
19. Vanoni MA, Curti B (2005) *Arch Biochem Biophys* 433:193–211.
20. Beinert H, Holm RH, Munck E (1997) *Science* 277:653–659.
21. Beinert H (2000) *J Biol Inorg Chem* 5:2–15.
22. Fontecave M (2006) *Nat Chem Biol* 2:171–174.
23. Studier FW (2005) *Protein Expression Purif* 41:207–234.
24. Otwinowski Z, Minor W (1997) *Methods Enzymol* 276:307–326.
25. Schneider TR, Sheldrick GM (2002) *Acta Crystallogr D* 58:1772–1779.
26. Brunger AT, Adams PD, Clore, GM, DeLano WL, Gros P, Grosse-Kunstleve RW, Jiang JS, Kuszewski J, Nilges M, Pannu NS, *et al.* (1998) *Acta Crystallogr D* 54:905–921.
27. Emsley P, Cowtan K (2004) *Acta Crystallogr D* 60:2126–2132.
28. Murshudov GN, Vagin AA, Dodson EJ (1997) *Acta Crystallog D* 53:240–255.
29. Laskowski RA, Macarthur MW, Moss DS, Thornton JM (1993) *J Appl Crystallogr* 26:283–291.
30. Wiley SE, Murphy AN, Ross SA, van der Geer P, Dixon JE (2007) *Proc Natl Acad Sci USA* 104:5318–5323.
31. Wiley SE, Paddock ML, Abresch EC, Gross L, van der Geer P, Nechushtai R, Murphy AN, Jennings PA, Dixon JE (2007) *J Biol Chem* 282:23745–23749.